Engineering Journal issn: 0125-8281

Article

Influence of Soaking Time on Deep Cryogenic Treatment of CuCoNiBe alloy

Nuwan Wannaprawat[1,2,a] **and Karuna Tuchinda**[1,2,b,*]

1 The Sirindhorn International Thai-German Graduate School of Engineering (TGGS), King Mongkut's University of Technology North Bangkok (KMUTNB), Bangkok 10800, Thailand
2 Material Manufacturing and Surface Engineering Research Centre (MaSE) Science and Technology Research Institute, King Mongkut's University of Technology North Bangkok (KMUTNB), Bangkok 10800, Thailand
E-mail: [a]nuwan.w-mesd2015@tggs.kmutnb.ac.th, [b,*]karuna.t@tggs.kmutnb.ac.th (Corresponding author)

Abstract. Deep cryogenic treatment (DCT) was investigated at different soaking times to determine the microstructural transformation and mechanical properties of copper beryllium (CuCoNiBe) alloy. Lattice shrinkage/distortion resulting from differences in thermal contraction/expansion between the α phase and γ phase caused internal stress, with large atomic dislocations leading to the formation of beryllides. Average beryllide size decreased with increasing DCT time by a maximum of 37% compared to non-DCT because new small beryllides were formed. Beryllides increased and distributed in the α phase with longer soaking time. Highest beryllide number and volume fraction found at the longest soaking time of 72 h were approximately 200% and 5%, respectively higher than for non-DCT. Increasing the number of beryllides played an important role in enhancing hardness and wear resistance. Maximal increase in hardness at 12% was observed for 72 h DCT, with reduction in wear volume of 30%. Residual stress as compressive stress showed high variation, with uneven distribution over the DCT sample. Impact strength of the DCT samples decreased by 50%. Analysis of fracture surfaces suggested that beryllide shape and beryllide at the grain boundaries played important roles in reducing fracture resistance. Thermal conductivity measurements of DCT-12 h and DCT-72 h samples indicated microstructural change, with the DCT-72 h sample recording a 2% drop in thermal conductivity compared to non-DCT.

Keywords: Deep cryogenic treatment, copper beryllium alloy, microstructure, thermal conductivity.

ENGINEERING JOURNAL Volume 26 Issue 4
Received 28 October 2021
Accepted 24 March 2022
Published 30 April 2022
Online at https://engj.org/
DOI:10.4186/ej.2022.26.4.25

1. Introduction

Copper beryllium (CuBe) alloys are widely used as industrial materials due to their unique combination of good electrical and thermal conductivity, outstanding resistance to corrosion, high strength and fatigue resistance [1-3]. Various applications include connector parts in electric circuits, spot welding electrodes, spring materials and mould casting. Commercial CuBe alloys contain small amounts of other metals that enhance performance such as Nickel (Ni), Co (Cobalt), Chromium (Cr), Zirconium (Zr) and Iron (Fe) [1-2, 4-6]. Adding these elements to CuBe alloys optimises strength, corrosion resistance and electrical/thermal conductivity, with the microstructure consisting of various precipitate types including Co beryllide and Ni beryllide [7].

Deep cryogenic treatment (DCT) is an effective method to improve material properties such as strength, hardness, wear-resistance and fatigue resistance. The process is a permanent treatment that offers dimensional or microstructural stability [8-10]. During DCT, the samples are subjected to low temperature of -196°C using a coolant medium as liquid nitrogen and liquid helium [10-11]. The DCT process improves mechanical properties and wear resistance of materials due to microstructural transformation, precipitation and removal of residual stress [12].

Previous studies have shown that cryogenic treatment can improve the properties of many materials including copper beryllium alloys. Wannaprawat et al. [13-14] studied the influence of DCT on the microstructure and material properties of CuBeZr alloy. Results showed that DCT improved CuBeZr alloy properties by increasing the number of NiZr precipitates and Ni precipitates. Hardness and wear resistance improved with increasing soaking time, while impact strength decreased because the precipitates concentrated along grain boundaries. Pervaz et al. [15-16] studied the effect of cryogenic treatment on CuBe2 at different soaking temperatures. They found that extensive cryogenic treatment at -186°C) refined grain size and increased the number of beryllides. Tensile strength improved due to refinement of the grain structure, while hardness also increased because the numbers of beryllide particles increased and were distributed in the matrix. Tribological properties of wear resistance improved significantly for all loading conditions. Yildiz et al. [17] investigated Be-Cu alloy that underwent cryogenic treatment. Results showed that electrical conductivity of the alloy increased because soaking at low temperatures increased the homogeneity of the crystal structure by dissolving the gaps and dislocations in alloy elements.

Here, CuCoNiBe alloy was subjected to deep cryogenic treatment. A wide range of soaking times from 0.5 h to 72 h was studied to better understand the effect of deep cryogenic treatment on microstructural transformation and changes in material properties. Different immersion times were investigated for microstructural transformation and residual stress, hardness, impact strength, wear-resistance and thermal conductivity. Results will be useful for optimal selection of DCT process time to improve engineering tools and components made from CuCoNiBe alloys. Understanding the effect of DCT time on CuCoNiBe alloy properties can be used as a guideline to improve material properties in the industrial engineering field.

2. Materials and Methods

The CuCoNiBe alloy (UNS C17510) used in this research was supplied by Grohe Siam Co., Ltd. Optical Emission Spectroscopy (OES) was used to determine the elemental composition of the CuCoNiBe alloy, with results shown in Table 1. Tensile strength, yield strength and elongation at 694 MPa ± 2.65, 552 MPa ± 3.06 and 18% ± 0.31 respectively were obtained from the tensile test. Deep cryogenic treatment (DCT) was performed in liquid nitrogen at - 196°C with different soaking times of 0.5 h, 1 h, 4 h, 8 h, 12 h, 16 h, 24 h, 48 h and 72 h. The samples were immersed in liquid nitrogen, removed immediately from the container when the desired immersion time was achieved and then left in the open air for 40 minutes until reaching room temperature (Fig. 1). A thermometer with thermocouple type K was used to monitor the temperature at the sample surface.

Optical microscopy (OM), Scanning Electron Microscopy - Energy Dispersive Spectroscopy (SEM-EDS) and X-ray Diffraction (XRD) were used to examine phase transformation and microstructural change in the samples. The sample surfaces were polished with different mesh sizes and then with 1 μm alumina powder. The surfaces were then etched with a solution of 5 g FeCl + HCl 50 ml + H_2O 50 ml for 5 s. Photography from OM and SEM was taken from 20 areas for each sample. A micrograph area of 1.7 μm^2 for each sample was used to determine precipitation amount and precipitate size by ImageJ program. All micrographs were converted to grayscale. The precipitates were shown as dark area in the images. Threshold of image intensity was automatically set by an application and precipitate area was analyzed using analyses. The area identified as precipitates was used to further determine volume fraction of precipitate and circular factor of precipitate shape. Grain size could also be estimated using Image J. The circular shape factor (CSF) was estimated from Eq. (1) [18-20].

$$\text{Circular shape factor} = \frac{4\pi A^2}{P} \quad (1)$$

where A is the precipitate area and P is the precipitate perimeter. Numerical values of the CSF indicated area shape as 0.9-1 sphere-shaped, 0.7-0.8 irregular sphere-shaped, 0.3-0.6 rod-shaped and 0-0.2 elongated [19]. Grain size was determined by the Jeffries Planimetric method (ASTM E112), while residual stress on surface specimens was investigated by a residual analyser (μ-X360 Residual Stress Analyser, Pulstec Industrial Co., Ltd.) using a chromium (Cr) X-ray tube at 30KV and 1.5 mA with 2 mm beam size following the cos α method. Ten points were examined on each specimen, as five points along

each of two horizontal lines from the left edge to the right edge, as shown in Fig. 2.

Table 1. Elemental composition (wt %) of the investigated CuCoNiBe alloy.

Element	CuCoNiBe alloy (wt %)
Cu	Bal.
Be	0.4 - 0.7
Ni	0.8 - 1.3
Co	0.3 - 1.3
Fe	Max 0.2

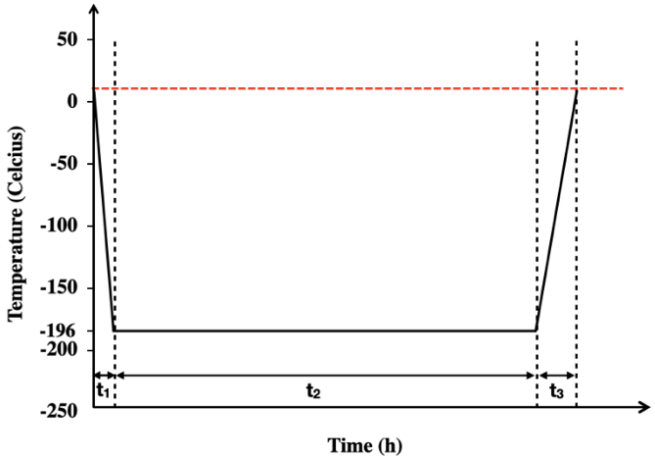

Remarks : t_1 : cooling time = 4s, t_2 : soaking time = 0.5 h, 1 h, 4 h, 8 h, 12 h, 16 h, 24 h, 48 h and 72 h, t_3 : warming time = 40 minutes

Fig. 1. Deep cryogenic treatment cycle for the CuCoNiBe alloy.

Vickers hardness results were measured using a 300 gf load and duration time of 15s with 20 measurement points for each sample. A Charpy Impact Testing Machine was used to perform the impact test with three repetitions for each condition. Samples were prepared following ASTM E23 and the fracture surface was subjected to SEM to analyse the effect of DCT at different soaking times.

Sliding wear tests were performed using a rotation ball on disk apparatus with tungsten carbide ball diameter of 6 mm. All experiments were performed under dry conditions at room temperature in ambient air with 10 N stationary constant loads and linear speed of 3 cm/s for 10,000 cycles. The samples were tested with three repetitions using the same sliding wear condition. Maximal Hertzian contact pressure was 1350 MPa. Wear volume was determined from the cross-section area of the wear track and its length on the sample surface. Ten measurements of wear track profile along the wear path were performed using a surface roughness tester and analysed by the ImageJ program.

Thermal conductivity was measured using a Laser Flash Apparatus (LFA 457, NETZSCH, LMS Instrument Co., Ltd., Thailand. The LFA tests were performed at 300 to 600°C selected from service temperatures for forming applications of CuCoNiBe alloy. However, only DCT samples at 12 and 72 h showed significant microstructure, i.e. precipitate number, size and location when compared with the non-DCT sample. Selected samples were prepared in a cylindrical shape with diameter of 12.5 mm and thickness 2.5 mm.

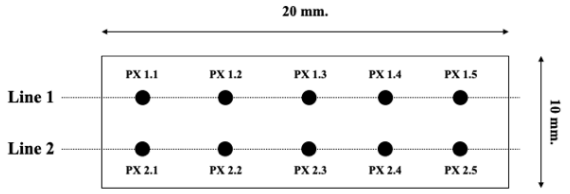

Fig. 2. Schematic of residual stress measurement points (PX).

3. Results and Discussion

3.1. Microstructural Analysis

3.1.1. Analysis of phase composition

Microstructures of non-DCT and DCT-72 h samples of CuCoNiBe alloy consisted of α matrix phase, shown as a light grey area, γ phase located at the grain boundaries shown as dark areas and beryllides shown as dark grey particles distributed in the α phase matrix (Fig. 3). The EDS results of non-DCT and DCT-72 h shown in Table 2 indicated that the α matrix phase was mainly composed of Cu with beryllide widely distributed in the α matrix phase composed of Be, Co and Ni. The γ phase contained Cu and was Be rich. However, Be could not be detected due to limitations of the SEM-EDS technique. Phase transformation was investigated using XRD analysis for non-DCT and DCT samples at 0.5 h, 48 h and 72 h, as shown in Fig. 4(a). Diffraction peaks showed that the main phase was α phase matrix, as shown on Cu (111), (200), (220) and (311), while the γ phase and beryllides were shown at 34.2° with low intensity (Fig. 4(b)). Diffraction peak results for all three DCT cases did not show the new phase, which might occur during the DCT process. The main peak of the α phase matrix on Cu (111) was shifted from 43.42° to 43.38° at DCT-48 h and DCT-72 h. The diffraction peak centres shifted towards lower 2 theta with longer soaking time, compared to non-DCT and DCT-0.5 h due to compressive strain or tensile strain developed in the lattice of CuCoNiBe alloy. Furthermore, the peak area of γ phase and beryllide showed enhanced intensity after longer DCT soaking time at 48 h and 72 h. The XRD analysis detected an increase in both precipitates due to transformation of the γ phase and beryllides in the α phase matrix.

3.1.2. Microstructural observation

Typical metallographic photographs of CuCoNiBe alloy non-DCT and DCT samples at different immersion times are shown in Fig. 5. The non-DCT condition consisted of

sphere-shaped, irregular-shaped (ellipsoid and irregular rod-like), rod-shaped and some large elongated beryllides. DCT at 0.5 h to 4 h showed increased irregular-shaped beryllides in the microstructure. Small beryllium spherical shapes also began to occur after DCT at 1h. For samples with DCT immersion time of 8 h to 72 h, more significant rod-shaped and irregular- shaped beryllides were seen, with beryllides also observed along grain boundaries. With increase in DCT soaking time above 0.5 h, beryllides with different sizes and shapes appeared along the grain boundaries and at triple junction grain boundaries.

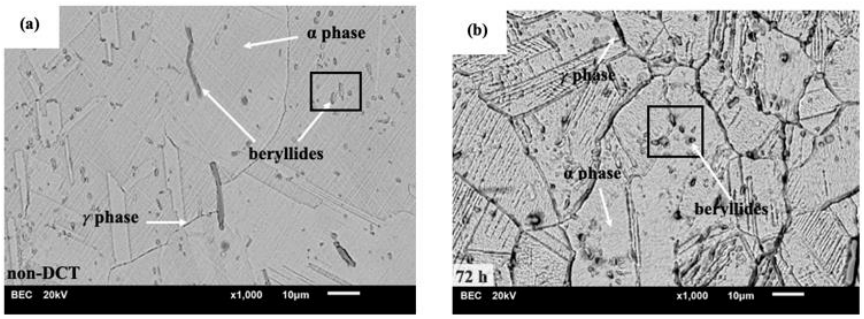

Fig. 3. Phase analysis by SEM with 1000X of (a) non-DCT and (b) DCT-72 h.

Table 2. Elemental composition (wt. %) of individual phases in CoCuNiBe alloy by SEM-EDS.

Sample	Microstructural phase	Elemental composition (wt. %)		
		Cu	Co	Ni
non-DCT	Beryllide	19.74	40.37	39.89
	α phase	98.75	0.76	0.65
DCT-72 h	Beryllide	20.11	40.87	39.02
	α phase	98.86	0.55	0.59

Microstructural changes due to the DCT process at different soaking times were investigated by micrographs, as shown in Fig. 6. Grain size, number and size and volume fraction of precipitates were plotted against the DCT soaking time and compared with non-DCT. Results showed that the DCT process did not affect grain size. Grain size of CoCuNiBe alloy averaged 30 μm to 35 μm (Fig. 6(a)), while Fig. 6(b) shows the average number of beryllides of non-DCT CuCoNiBe alloy as 137±29 particles in an area of 1.7 μm^2. The number of beryllides gradually increased after the DCT process at more than 1 h and then remained steady from 12 h to 48 h. Maximal value found at the longest soaking time of 72 h was 200% higher than the non-DCT case. Average beryllide size at different soaking times decreased 37.5% from 8 μm to 5 μm compared with non-DCT and DCT-8 h and then remained constant from DCT-12 h to 72 h (Fig. 6(b)). The volume fraction of beryllide for non-DCT and DCT samples at different soaking durations was estimated, as shown in Fig. 6(c). Volume fraction increased gradually from DCT-0.5 h to 24 h and then remained steady at nearly 5%.

The mechanism of beryllide precipitation by deep cryogenic treatment is explained as follows. Microstructural transformation could occur during DCT process, i.e. cooling down and warming up period, because of the diverse thermal expansion/contraction between the α phase, γ phase and beryllides producing lattice shrinkage and distortion. These effects induced high internal stress, generating a large number of dislocations that further contributed to beryllide clusters [21]. These stresses forced more Co, Ni and Be atoms to move to nearby crystal defects, leading to the formation of more beryllide clusters. Consequently, during the warm-up process from - 196°C to room temperature, these beryllide clusters transmuted into beryllides and increased the number of beryllides, while the remaining beryllides altered gradually in size. At longer immersion time, the volume and size of beryllides increased. The structure was further distorted and more Co, Ni and Be atoms were conveyed to beryllide clusters and beryllides. This phenomenon has also been observed and discussed in other works where effect of soaking time for steel materials were investigated [22-23].

In the OM micrographs, beryllides can be distinguished by circular shape factor (CSF) and the evaluation of CSF as -sphere-shaped (0.9-1), irregular-shaped (0.7-0.8), rod-shaped (0.3-0.6) and elongate (0-0.2) are given in Topic 2. Numerical values of CSF of non-DCT showed sphere-shaped, irregular-shaped and rod-shaped with some elongated. After the DCT process, numerical values of CSF showed that the percentage of irregular-shaped and rod-shaped beryllides increased, as shown in Fig. 7 (b) to (j). The rod-shaped percentage increased continuously in the microstructure with increasing immersion times. However, when considering

individual results, the CSF of each condition showed fluctuating results of beryllide shapes. New beryllide clusters initially gathered into beryllide sphere-shapes, while the remaining beryllides commuted from sphere-shaped to irregular-shaped and rod-shaped at longer soaking times. An increasing amount of sphere-shaped beryllides was caused by cumulative clusters that gradually led to further precipitation of new beryllides, resulting in increased amounts of sphere-shaped beryllides at longer soaking times.

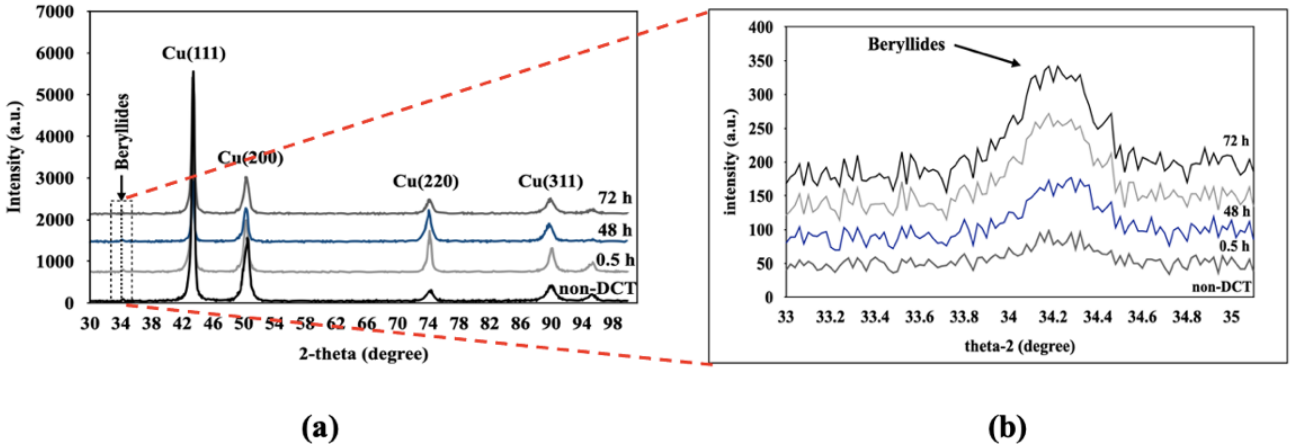

Fig. 4. XRD patterns of (a) CuCoNiBe alloy and (b) showing beryllide precipitate.

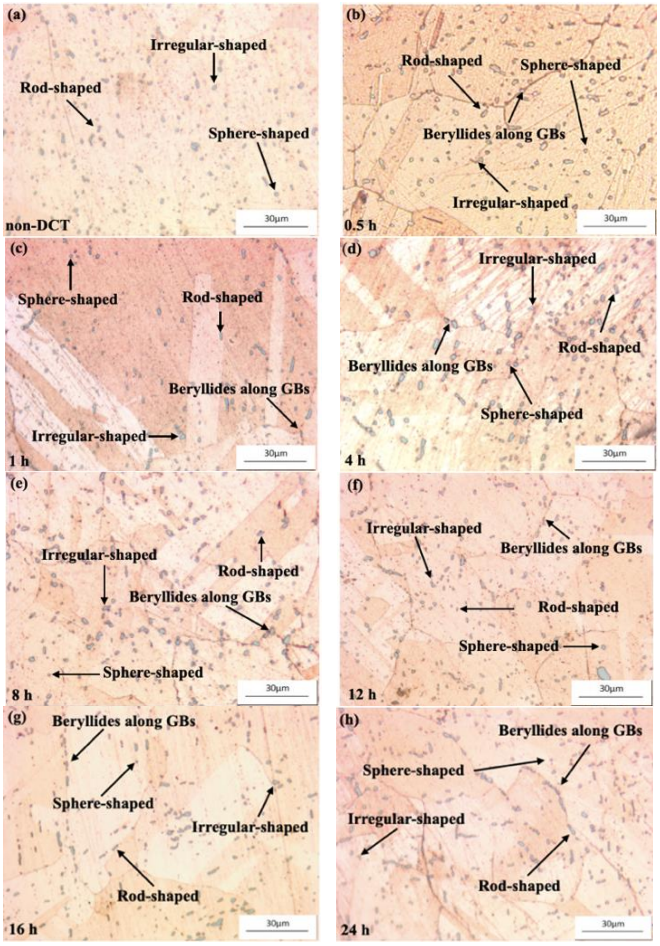

Fig. 5. Metallographic photographs (a) non-DCT, (b) 0.5 h, (c) 1 h, (d) 4 h, (e) 8 h, (f) 12 h, (g) 16 h, (h) 24 h, (i) 48 h and (j) 72 h.

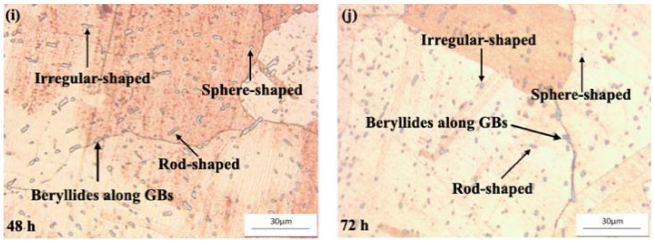

Fig. 5. Continued.

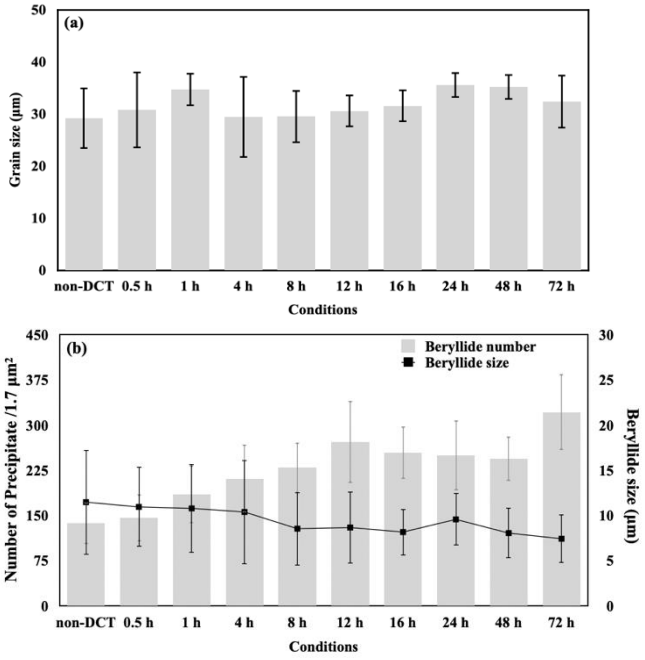

Fig. 6. Relationship of DCT soaking time with (a) grain size, (b) number of precipitates and precipitate size and (c) volume fraction of precipitates of CuCoNiBe alloy.

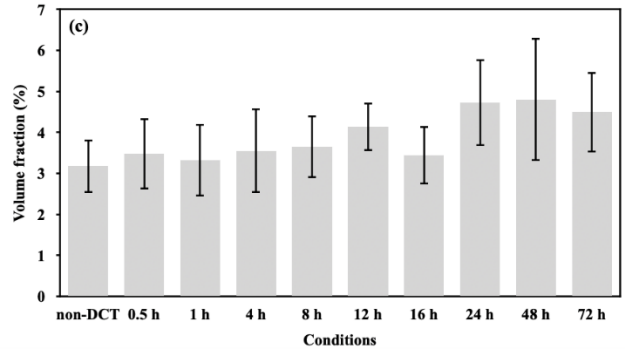

Fig. 6. Continued.

Results showed an increase in irregular-shaped and rod-shaped beryllides with increasing immersion time, caused by lattice misfits that generated stress due to differing thermal expansion/contraction between the α phase, γ phase and beryllides. Misfit stress is determined by misfit strain and moduli that influence microstructural evolution and impact precipitate shape and precipitate coarsening [24]. Thus, internal stress developed in different directions and induced misfit strain on the microstructure.

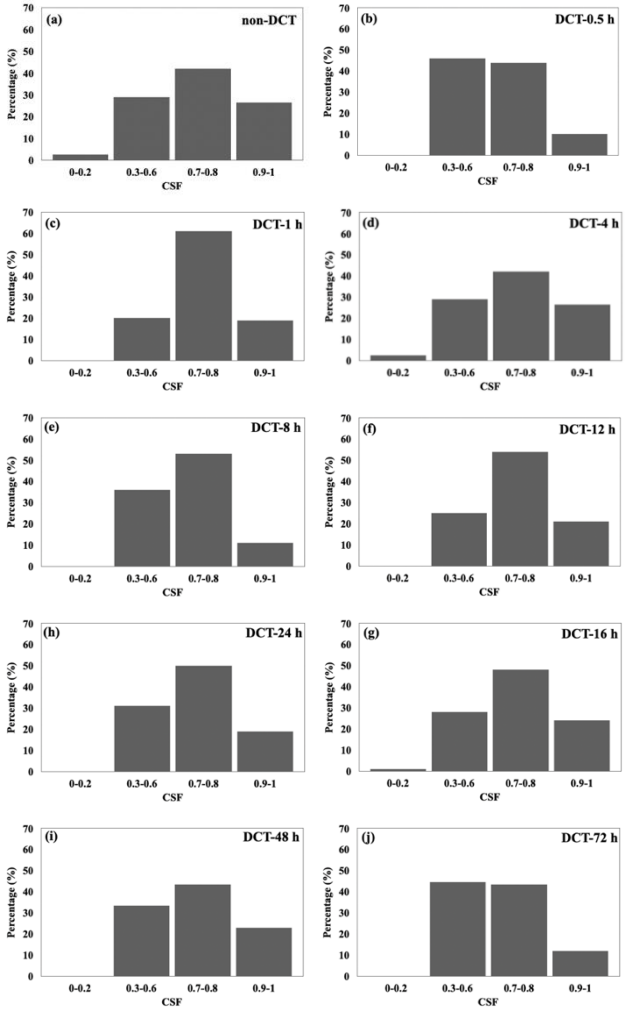

Fig. 7. Circular shape ratio (a) non-DCT, (b) 0.5 h, (c) 1 h, (d) 4 h, (e) 8 h, (f) 12 h, (g) 16 h, (h) 24 h, (i) 48 h and (j) 72 h.

3.2. Residual Stress

Residual stress was investigated on samples that showed significant change in the number of beryllides, i.e. DCT at 12 h, 24 h, 48 h and 72 h with results plotted against DCT time together with non-DCT. Results of average residual stress showed compressive residual stress for all cases, as shown in Fig. 8. Residual stress of non-DCT had an average value of 252.3±20.17 MPa. However, approximately 70% of non-DCT areas could not be measured for residual stress because the diffraction spectra did not provide a complete Debye ring, as shown in Fig. 9(a). On the other hand, 100% of the testing points of selected DCT samples generated complete Debye rings in all areas, as shown in Fig. 9(b). This suggested that differences in crystal orientation did not produce a diffraction spectrum for non-DCT samples, while the microstructure of selected DCT samples had a more uniform phase distribution that could be obtained by a complete Debye ring. Three specimens for each condition were measured, with 10 testing points for each specimen (30 total testing points). Average values of residual stress were distributed unevenly over the whole specimen in all conditions with high variation from three specimens, as shown in Table 3. Various compressive residual stress levels developed and were distributed in different areas, leading to dislocation and microstructural transformation [14, 24].

As mentioned above, average residual stress of DCT samples showed compressive residual stress with high variation that increased with immersion time. This increase in compressive residual stress enhanced material hardness properties and delayed crack initiation and crack growth leading to improved wear resistance. Similar observations were recorded by Wannaprawat [14] and Kara [25]. Maximal compressive residual stress at DCT-24 h was 295.80±90.13 MPa, an increase of 17% compared with non-DCT. However, the compressive residual stresses tended to decline significantly after DCT with 48 h and 72 h by approximately 16% and 25%, respectively, in results compared with DCT-24 h. After DCT, beryllides and the γ phase formed at grain boundaries and in the α matrix phase because and the phases had different thermal and elastic properties that induced internal stress and atomic dislocation in the microstructure. The lattice volume of beryllide increased during microstructural transformation, causing residual stress in the materials that induced compressive or tensile stress by lattice contraction/expansion surrounding the structure. Formation of beryllide was enhanced by compressive stress after DCT. Compressive residual stress increased at higher beryllide volume fractions. This agreed with the XRD results showing the peak of precipitates with increasing beryllide intensity, while the volume fraction of beryllide also showed increased beryllide content.

The variation in residual stress value was noticeably high for all DCT conditions, indicating the existence of various stress levels developed in different areas, as shown

in Fig. 8 and Table 3. Results suggested that beryllides were distributed unevenly over DCT samples and induced compressive residual stress or tensile residual stress in different areas. The DCT process caused diverse defects such as lattice shrinkage and atomic dislocation that resulted in microstructural transformation of beryllides and the γ phase. On the other hand, compressive residual stress declined significantly after DCT-48 h. suggesting that at longer soaking times, beryllides and new beryllide clusters gathered and became larger. This behaviour led to decrease of Be, Co and Ni atoms in the α matrix phase at longer soaking times because Be atoms combined with other elements to form beryllides and were located along the grain boundaries (γ phase). Therefore, the α matrix phase lattice was transformed into a pure copper lattice in some areas, leading to reduced average compressive residual stress. This result concurred with a shift in the main copper diffraction peak of DCT-48 h and DCT-72 h as the Be atoms were ejected from the α matrix phase to the grain boundaries, concurring with Pervaz et al. [15]. Thus, crystallinity of the α matrix phase increased after DCT and formation of the α matrix phase promoted tensile residual stress. Precipitate transformation was associated with the development of residual stress in DCT samples and related to increased impact strength.

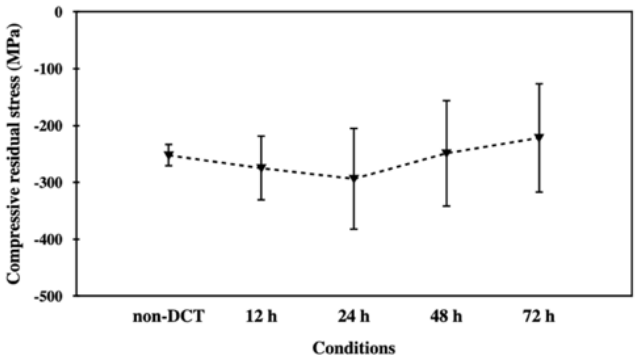

Fig. 8. Residual stress of CuCoNiBe alloy for non-DCT and DCT at different soaking times.

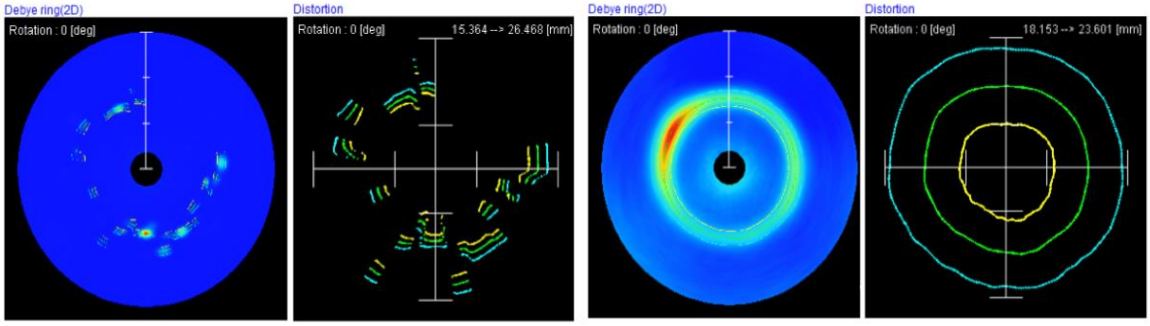

(a) (b)

Fig. 9. Debye rings from non-DCT measurement obtained using a μ-X360 residual stress analyser: (a) incomplete Debye ring result, (b) complete Debye ring result.

Table 3. Distribution of residual stress in non-DCT and DCT specimens for different measuring points.

Sample	Point / Line	PX1	PX2	PX3	PX4	PX5
Non-DCT	1	-261 MPa	-243 MPa	NA	-276 MPa	-230 MPa
	2	-308±45 MPa*	NA	-196 MPa	-305 MPa	-291±25 MPa*
DCT-12 h	1	-254±66 MPa	-251±92 MPa	-248±53 MPa	-254±57 MPa	-304±28 MPa
	2	-302±49 MPa	-305±74 MPa	-268±17 MPa	-235±78 MPa	-323±23 MPa
DCT-24 h	1	-321±57 MPa	-313±22 MPa	-369±145 MPa	-310±129 MPa	-256±47 MPa
	2	-319±173 MPa	302±110 MPa	-291±41 MPa	-303±13 MPa	-225±14 MPa
DCT-48 h	1	-295±21 MPa	-282±32 MPa	-276±40 MPa	-265±119 MPa	-240±125 MPa
	2	-272±192 MPa	-238±82 MPa	-247±125 MPa	-217±95 MPa	-152±61 MPa
DCT-72 h	1	-157±61 MPa	-259±187 MPa	-166±61 MPa	-222±49 MPa	-244±183 MPa
	2	-322±91 MPa	-202±101 MPa	-218±57 MPa	-206±40 MPa	-217±58 MPa

Remarks: 1. X is line number. 2. The residual stress measurement could be obtained from * as 1 specimen only.

3.3. Hardness Test and Wear Test

The influence of DCT at different soaking times on hardness and wear volume of the CuCoNiBe alloy is presented in Fig. 10. Average values for hardness were significantly higher, with lower wear volume than non-DCT. Hardness of the DCT sample increased continuously with increasing soaking time, with optimal

hardness of 320±7.5 HV obtained at DCT-72 h (12% higher compared to non-DCT). Wear volume of DCT samples decreased as soaking time increased. Wear volume of DCT-72 h showed improvement, with 30% lower wear volume compared to the non-DCT sample. There was a general corelation between hardness and wear volume. When hardness increased, wear volume decreased. This was associated with the transformation of precipitates (hard phase) produced during the DCT process (cooling down and warming up). Results suggested that increased precipitation of beryllides, increase in the number and volume fraction of beryllides and decrease in size of beryllides embedded in the α matrix phase had a major effect on hardness and wear properties because the hardness of beryllide was higher than the α matrix phase. Increased DCT soaking time improved the hardness and wear properties of CuCoNiBe alloy through further structural distortion that led to the formation of more beryllides at crystal defects. The OM micrographs showed that the number of beryllides for DCT-72 h increased remarkably to 200% higher than non-DCT and were distributed more uniformly on the α matrix phase compared with non-DCT. Increase in the number of hard phases led to enhancement of hardness and wear resistance, which was also found in CuBe alloys and other materials [13-14, 25-29].

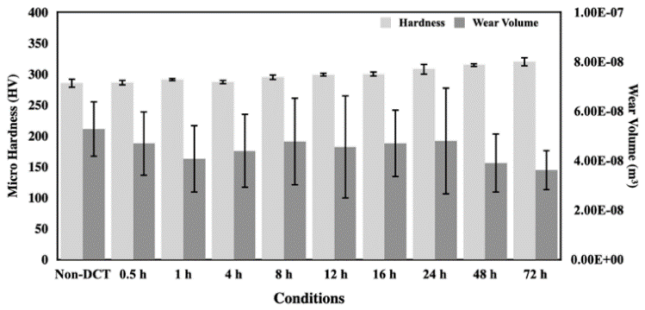

Fig. 10. Hardness and wear volume of non-DCT and DCT-treated CoCuNiBe alloy.

3.4. Impact Testing and Fracture Surface

Impact strength testing results of CuCuNiBe alloy (performed according to the Charpy V-notch test) are presented as impact strength variation against different soaking times in Fig. 11. Impact strength of non-DCT had an average value of 5,125±125J/m. However, average impact strength at DCT-0.5 h to DCT-72 h reduced significantly by approximately 50%. Fracture surface micrographs are presented in Fig. 12. Fracture surfaces of all samples showed a combination of failure types consisting of cleavage facets, dimples, tear ridges, cracks and beryllide cracks. Dimples presented the highest area of fracture surface in all cases. Beryllide cracks were easily observed in the SEM micrographs. To confirm these cracks, beryllide cracks at DCT-72 h were subjected to SEM-EDS mapping, as shown in Fig. 13. The portion of beryllide cracks increased at longer soaking times, while above DCT-16 h the number of cracks increased, as shown in Fig. 12 (h) to (j).

Generally, the fracture toughness of alloys is impacted by precipitate number, precipitate size and grain refinement. Results showed that all cases had similar values for average grain size. As discussed under microstructural observations, precipitation hardening, which occurred during the DCT process, enhanced impact toughness since the strengthening effect in treated samples mainly resulted from beryllides that inhibited dislocation movement. In treated samples the size of beryllides decreased, while numbers of beryllides increased with increasing soaking time. These changes did not enhance fracture toughness. Hence, the analysis results suggested that beryllide shapes and locations at the grain boundaries had an important effect on fracture toughness. Yuan et al. [30] noted that rod-shaped precipitates exhibited lower fracture toughness. The CSF ratios of DCT samples showed that the incremental CSF ratio of rod-shaped beryllides increased with increasing immersion time. Increase in rod-shaped beryllides with reduction in impact strength related to lattice misfits because rod-shaped beryllides were generated by lattice misfits due to different thermal contraction/expansion between phases, inducing different misfit stress and strain on the microstructure. Small sphere-shaped beryllide clusters inhibited dislocation movement [31-32] and compiled on the α matrix phase with increasing soaking time. CSF results also showed that increase in sphere-shaped amounts at longer soaking times did not enhance DCT sample impact properties. Beryllides tended to accumulate along grain boundaries with increasing soaking time. Thus, beryllides at the grain boundaries also caused deterioration of impact strength.

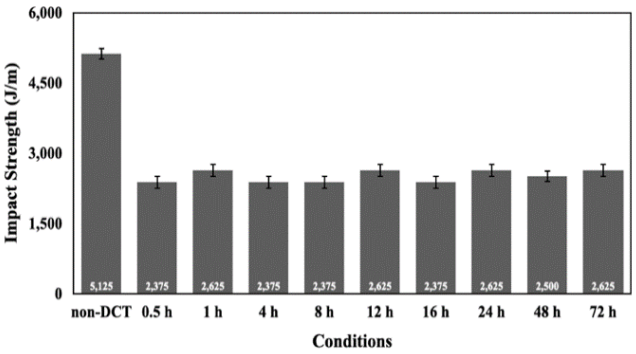

Fig. 11. Impact test results of non-DCT and DCT-treated CoCuNiBe alloy.

This study also found that CuCoNiBe alloy after the DCT process with longer soaking time introduced the stage of tensile residual stress that was expected to degrade impact properties. High variation in residual stress was observed with different levels of residual stress developed throughout the samples. These changes suggested that the reason for decrease in impact strength related to beryllide shapes, beryllide at grain boundaries and residual stress.

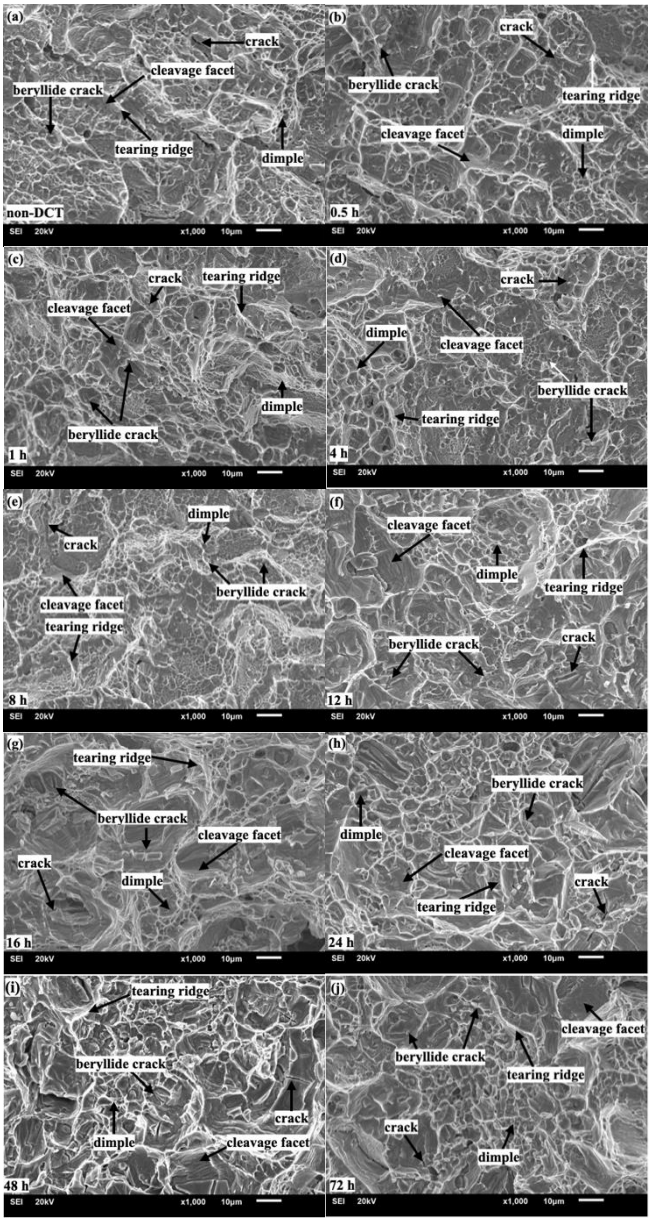

Fig. 12. Fracture surface of CoCuNiBe alloy: (a) non-DCT, (b) 0.5 h, (c) 1 h, (d) 4 h, (e) 8 h, (f) 12 h, (g) 16 h, (h) 24 h, (i) 48 h and (j) 72 h.

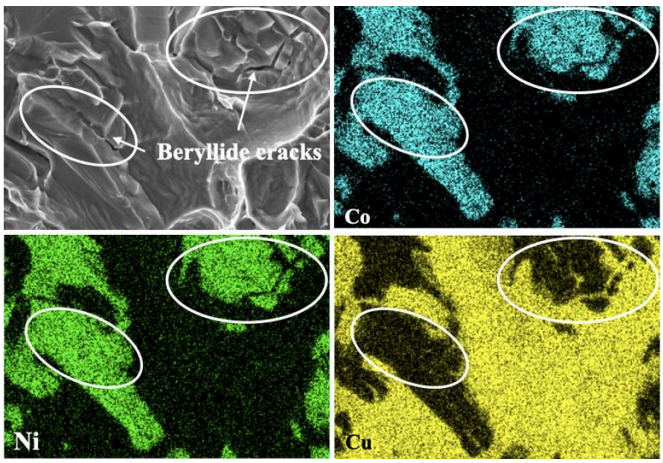

Fig. 13. SEM-EDS mapping of beryllide cracks on the fracture surface of DCT-72 h treated CuCoNiBe alloy.

3.5. Thermal Conductivity

Thermal conductivity results (performed according to LFA methods) are shown in Fig. 14. Temperature change during the DCT process suggested that the effect of lattice mismatch was caused by thermal contraction and expansion between different phases that influenced charge transport due to lattice misfit, defect, and misfit dislocation [24]. Such defects then degraded thermal conductivity. Beryllides were located along the grain boundaries and distributed in the microstructure and this affected the thermal conductivity of DCT-treated samples. Thermal conductivity testing performed on non-DCT and samples prepared under DCT conditions of 12 h and 72 h showed significant changes in microstructure, i.e. beryllide number, size and locations. Thermal conductivity of the CuCoNiBe alloy was tested at temperatures between 300°C and 600°C as typical temperature ranges for casting. Results of DCT samples were compared with the non-DCT value. Average thermal conductivity of the DCT samples showed maximal difference of 2% compared with non-DCT. Results suggested that the DCT process did not impact thermal conductivity of CuCoNiBe alloy.

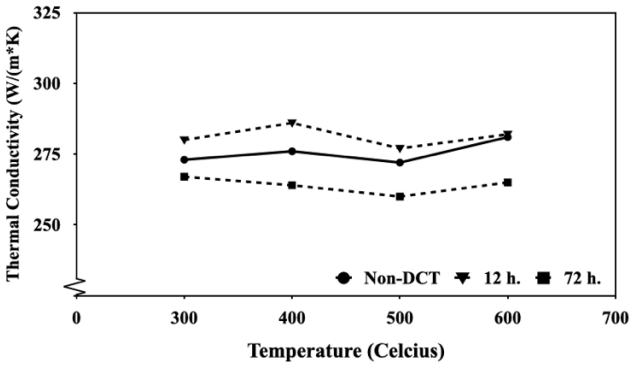

Fig. 14. Thermal conductivity of non-DCT and DCT CuCoNiBe alloy.

4. Summary

Effects of DCT applied for 0.5 h, 1 h, 4 h, 8 h, 12 h, 16 h, 24 h, 48 h and 72 h were investigated on microstructure, residual stress, hardness, wear resistance and impact strength of CuCoNiBe alloy, with conclusions summarised as follows:

- Microstructural observations showed that beryllide transformation occurred during the DCT process (cooling down and warming up) due to thermal contraction/expansion of different phases (α phase, γ phase and beryllides). The DCT process increased the number and volume fraction of beryllides in the α matrix at longer soaking times. Maximal increaser in numbers of beryllides at 200% was observed at 72 h DCT with a 5% increase in beryllide volume fraction.

- Residual stress for all samples was found to be compressive residual stress, with high variation unevenly distributed over the DCT samples. Maximal compressive residual stress was found in DCT-24 h, with a 17% increase compared to the non-DCT sample, while compressive residual stresses of DCT-48 h and DCT-72 h reduced by 16% and 25% respectively compared to DCT-24 h. The reduction of compressive residual stress was associated with Be, Co and Ni atoms concentrating in the α matrix phase as a result of the transformation of beryllides that impacted the α matrix phase at longer soaking durations.
- Hardness and wear resistance improved with longer DCT. Number and volume of precipitates (harder phase) increased in the α phase with longer soaking time. These changes resulted in a major increase in hardness and wear resistance. Maximal hardness increased by 12%, with a 30% reduction in surface sliding wear at DCT-72 h.
- Results of impact strength of CuCoNiBe alloy showed a sudden decrease by approximately 50% for all DCT-treated samples. Analysis of the fracture surfaces suggested that beryllide locations along the grain boundaries induced more precipitate cracks.
- The DCT-12 h and DCT-72 h samples were selected for thermal conductivity testing due to their major microstructural transformation. Lattice defects occurred in the microstructure that degraded the thermal conductivity of DCT-treated samples. The selected DCT samples showed minor differences in thermal conductivity, with a 2% increase at 12 h and 72 h soaking time compared to the non-DCT sample. Thus, results showed no degradation of thermal conductivity for DCT samples compared to the non-DCT sample.

Acknowledgement

This research was funded by King Mongkut's University of Technology North Bangkok (KMUTNB) (Contract no. KMUTNB-61-GOV-01-54). The authors also wish to thank Grohe Siam Co., Ltd. for their joint support through the Research and Researchers for Industries (RRI) Ph.D. Programme (Contract no. PHD59I0070).

References

[1] G. F. Vander Voort, "Metallography and microstructures of nonferrous alloys, metallography and microstructures of beryllium, copper-beryllium, and nickel-beryllium alloys," in *ASM Handbook: Metallography and Microstructures*. USA: ASM International, 2004, vol. 9, pp. 752–760.

[2] D. J. Chakrabarti, D. E. Laughlin, and L. E. Tanner, "The Be–Cu (Beryllium copper) system," *Bulletin of Alloy Phase Diagrams*, vol. 8, no. 3, pp. 269–288, 1987.

[3] N. J. Simon, E. S. Drexler, and R. P. Reed, "Beryllium Copper," in *Properties of Copper and Copper Alloys at Cryogenic Temperatures*. New York, United States: National Institute of Standards and Technology Monograph, 1992, vol. 177, pp. 9.1-15.36.

[4] J. R. Davis, "Metallurgy, alloys, and applications," in *Copper and Copper Alloys*. USA: ASM International, 2001, pp. 1-102.

[5] L. Collini, *Alloys Early Applications and Current Performance—Enhancing Processes*. Intechopen, 2012. *Copper* [Online]. Available: https://www.intechopen.com/books/1454

[6] R. Konečná and S. Fintová, *Copper and Copper Alloys: Casting, Classification and Characteristic Microstructures*. Intechopen, 2012. [Online]. Available: https://www.intechopen.com

[7] Y. C. Tang, Y. L. Kang, L. J. Yue, and X. L. Jiao, "The effect of aging process on the microstructure and mechanical properties of a Cu-Be-Co-Ni alloy," *Mater. Des.*, vol. 28, no. 3, pp. 332-341, 2015

[8] G. Ventura and L. Risegari, *The Art of Cryogenics Low Temperature Experimental Techniques*, 7th ed. Amsterdam: Elsevier, 2008.

[9] D. T. Klaus and R. Richard, *Cryogenic Engineering-Fifty Years of Progress*, 1st ed. New York: Springer-Verlag New York, 2007.

[10] D. Thakur, B. Ramamoorthy, and L. Vijayaeaghavan, "Influence of different post treatments on tungsten carbide–cobalt inserts," *Mater. Lett.*, vol. 62, pp. 4403-4406, 2008.

[11] J. C. Harkness and A. Guha, "Metallography and microstructures of beryllium, copper-beryllium, and nickel-beryllium alloys," *ASM Handbook*. USA: ASM International, 2004, vol. 9.

[12] Y. Choa, Y. Wang, D. Sang, Y. Li, R. Fu, and X. Zhang, "Effects of deep cryogenic treatment on the microstructure and mechanical properties of commercial pure zirconium," *J. Alloys Compd.*, vol. 619, pp. 513-519, 2015.

[13] N. Wannaprawat and K. Tuchinda, "Study of deep cryogenic treatment process effect on microstructure and properties of CuBeZr alloy," *KEM*, vol. 841, pp. 335–339, May 2020.

[14] N. Wannaprawat and K. Tuchinda, "Influence of deep cryogenic treatment on microstructure, hardness, impact strength and wear of CuBeZr alloy," *Chiang Mai J. Sci*, vol. 48, no. 2, pp. 631-647, 2021.

[15] A. M. Pervaz, J. H. Siddhi, M. S. Rasool, and A. Rajadurai, "Effect of cryogenic treatment on microstructure and properties of CuBe2," *Metallogr. Microstruct. Anal.*, vol. 5, pp. 528–535, 2016.

[16] A. M. Pervaz and J. H. Siddhi, "Enhancing wear resistance of cryo treated Cu-Be2 alloy," *Silicon*, vol. 11, pp.105–115, 2019.

[17] Y. Yildiz, M. M. Sundaram, K. P. Rajurkar, and M. Nalbant, "The effects of cold and cryogenic treatments on the machinability of beryllium-copper alloy in electro discharge machining," in *The 44th CIRP Conference on Manufacturing Systems*, Madison, WI, USA, 2011.

[18] V. Alan and V. Milan, "Correlation between shape factor and mechanical properties of graphitic cast irons," *Prod. Eng. Arch.*, vol. 11, no. 2, pp.11-14, 2016.

[19] N. A. Miller and J. J. Henderson, "Quantifying sand particle shape complexity using a dynamic, digital imaging technique," *Agron. J.*, vol. 102, pp. 1407–1414, 2010.

[20] R. Y. Zhang, H. L. Qin, Z. N. Bi, J. Li, S. Paul, T. L. Lee, S. Y. Zhang, J. Zhang, and H. B. Dong, "Temperature-dependent misfit stress in gamma double prime strengthened Ni-base superalloys," *Metall Mater Trans A*, vol. 51, pp. 1860-1873, 2020.

[21] X. Guoliang, W. Qiangsong, M. Xujun, X. Baiqing, and P. Lojun, "The precipitation behaviour and strengthening of a Cu-2.0 wt.% Be alloy," *Mater. Sci. Eng. A*, vol. 558. pp. 326-330, 2012.

[22] K. Amini, A. Akhbarizadeh, and S. Javadpour, "Investigating the effect of holding duration on the microstructure of 1.2080 tool steel during the deep cryogenic heat treatment," *Vacuum*, vol. 86, no. 10, pp. 1534-1540, 2012.

[23] D. Das, A. K. Dutta, and K. K. Ray, "Influence of varied cryo treatment on the wear behavior of AISI D2 steel," *Wear*, vol. 266, no. 1–2, pp. 297-309, 2009.

[24] G. R. Li, J. F. Cheng, H. M. Wang, and C. Q. Li, "The influence of cryogenic-ageing circular treatment on the microstructure and properties of aluminium matrix and composites," J. Alloys Compd., vol. 695, pp. 1930-1945, 2007.

[25] F. Kara, O. Ӧzbek, N. A. Ӧzbek, and Ĭ. Uygur, "Investigation of the effect of deep cryogenic process on residual stress and residual austenite," *Gazi Journal of Engineering Sciences*, vol. 7, no. 2, pp. 143-151, 2021.

[26] A. Çiçek, E. Ekici, T. Kıvak, F. Kara, and N. Uçak, "Performance of multilayer coated and cryo-treated uncoated tools in machining of AISI H13 tool steel—Part 2: HSS end mills," *J. of Materi Eng and Perform*, vol. 30, pp. 3446–3457, 2021.

[27] M. Kam, "Effects of deep cryogenic treatment on machinability, hardness and microstructure in dry turning process of tempered steels," *Proc. Inst. Mech. Eng. E*, vol. 235, vol. 4, pp. 927–936, 2021.

[28] J. H. Tylczak and A. Oregon, "Abrasive wear," in *ASM Handbook Volume 18: Friction, Lubrication and Wear Technology*. USA: ASM International, 1992, pp. 184-190.

[29] F. Kara, M. Karabatak, M. Ayyıldız, and E. Nas, "Effect of machinability, microstructure and hardness of deep cryogenic treatment in hard turning of AISI D2 steel with ceramic cutting," *J. Mater. Res. Technol.*, vol. 9, no. 1, pp. 969-983, 2020.

[30] S. P. Yuan, R. H. Wang, G. Liu, J. M. Park, J. Sun, and K. H. Chen, "Effect of precipitate morphology on the notch sensitivity of ductile fracture in heat-treatable aluminium alloys," *Mater. Sci. Eng. A*, vol. 517, pp. 7369-7381, 2010.

[31] Y. Zhao, C. C. Wang, X. Wang, J. C. Huang, G. F. Zhang, M. T. Wang, Z. C. Zhang, and M. Wu, "Effects of precipitation behaviours on the microstructure and fracture toughness of Al-Cu-Mg aluminium alloys," *Optoelectron. Adv. Mater. Rapid Commun.*, vol. 10, no. 7-8, pp. 583 – 589, 2016.

[32] H. Somekawa, A. Singh, and T. Mukai, "Effect of precipitate shapes on fracture toughness in extruded Mg–Zn–Zr magnesium alloys," *J. Mater. Res. Technol.*, vol. 22, pp. 965–973, 2007.

DOI:10.4186/ej.2022.26.4.25

Nuwan Wannaprawat received B.Eng. and M.Eng. degree in material engineering from King Mongkut's University of Technology Thonburi (KMUTT), Thailand, in 2012 and 2015. She received Ph.D in Mechanical Engineering (International Program) from The Sirindhorn International Thai-German Graduate School of Engineering (TGGS), Mongkut's University of Technology North Bangkok (KMUTNB), Thailand, in 2021. Her research was funded by King Mongkut's University of Technology North Bangkok (KMUTNB) (Contract no. KMUTNB-61-GOV-01-54) and Research, Researchers for Industries (RRI) Ph.D. Programme (Contract no. PHD59I0070). Her research interests focus on material processing using cryogenic treatment and material characterization.

Karuna Tuchinda received B.Eng. and Ph.D degree in mechanical engineering at Imperial College London, U.K. with the Royal Thai Government Scholarship. In 2002, she started working as Lecturer at Department of Tool and Material Engineering, Faculty of Engineering, King's Mongkut University of Technology Thonburi (KMUTT), Bangkok, Thailand. Since 2015, she has worked as Lecturer and Researcher in Mechanical Engineering Simulation and Design (MESD) Group at The Sirindhorn International Thai-German Graduate School of Technology (TGGS), King Mongkut's University of Technology North Bangkok (KMUTNB). Her research interests are Computational mechanics and finite element modeling, Material mechanical behaviour and failure, Mechanics of thin films and coatings, Material characterization and Processing and modelling.